

Effects of broken time-reversal symmetry on transmission zeros in the Aharonov-Bohm interferometer

Tae-Suk Kim

Institute of Physics and Applied Physics, Yonsei University, Seoul 120-749, Korea

Sam Young Cho and Chul Koo Kim

*Institute of Physics and Applied Physics, Yonsei University, Seoul 120-749, Korea
and Center for Strongly Correlated Materials Research, Seoul National University, Seoul 151-742, Korea*

Chang-Mo Ryu

Department of Physics, Pohang University of Science and Technology, Pohang 790-784, Korea

(Received 19 October 2001; published 3 June 2002)

In this paper, we study the behavior of the transmission zeros in the closed Aharonov-Bohm (AB) interferometer with an embedded scattering center in one arm and the corresponding change in the transmission phase when the time-reversal symmetry is broken by magnetic fields. Specifically, we consider three embedded scattering centers: one discrete energy level, a double-barrier well, and a t stub. We find the following from our model study: (i) The transmission zeros are real when the AB flux is an integer or a half integer multiple of the flux quantum, and the transmission phase jumps by π at the zeros. (ii) The transmission zeros become complex or are shifted off the real-energy axis when the magnetic AB flux is not an integer or a half integer multiple of the flux quantum, and the transmission phase evolves continuously. (iii) The distance of the zeros from the real-energy axis or the imaginary part of the transmission zeros is sinusoidal as a function of the magnetic AB phase. We suggest the experimental setup which can test our results.

DOI: 10.1103/PhysRevB.65.245307

PACS number(s): 73.23.-b, 73.50.Bk, 73.63.Nm

I. INTRODUCTION

Recent advances in nanotechnology have made it possible to measure the phase of electron wave function.¹⁻⁵ In bulk systems, phase coherence of electron wave functions can be washed out by inelastic scattering processes. On the other hand, the phase of electron wave function can be preserved in nanoscopic systems. Typical experimental tools, which can measure the electron's phase, are the Aharonov-Bohm (AB) interferometers. To study the phase evolution due to the target system, the system is inserted in one of two arms of the AB interferometer. The I - V curves are measured between the external electrodes connected to the AB ring as function of the AB magnetic flux while other control parameters, e.g., the Fermi energy level, are varied. The phase evolution of the electron wave functions in the target system is extracted from the measured I - V curves.

The closed AB interferometer in a two-terminal configuration does not yield much information about the phase shift in the target system due to the phase locking effect.^{6,7} Multiple windings of the electron motion along the AB ring result in the conductance which is even^{6,7} in the AB flux Φ or $G(-\Phi) = G(\Phi)$. This Onsager relation⁸ constrains the measured phase to be either 0 or π . This phase locking effect can explain the observed phase jump by π at the conductance peaks¹ of the closed AB interferometer with an embedded quantum dot. The same phase of the transmission amplitude was observed¹ at successive Coulomb peaks. This means that an additional phase shift by π should occur in between two successive Coulomb peaks. The existence of the transmission zeros can also explain this feature.^{9,10}

In order to observe the phase evolution in the target system, an open AB interferometer was devised by Schuster *et al.*,² which is similar to the double-slit experiments. Suppression of the backscattered electrons prevents the multiple windings along the AB ring so that the total transmission amplitude becomes the sum of two transmission amplitudes through the upper and lower arms,

$$t = t_l + t_u e^{i\phi}. \quad (1)$$

Here ϕ is the AB phase due to the magnetic flux. Measuring the conductance which is proportional to $|t|^2$ as function of the AB phase, the transmission phase of the target system can be directly obtained.

In a phase-coherent system, the two different phases can be defined. The Friedel phase θ_f is defined as the argument of the determinant of the scattering S matrix, $e^{2i\theta_f} = \det S$. The change in the Friedel phase is related to the density of states via the Friedel sum rule,¹¹ $\rho(E) = \pi^{-1} d\theta_f/dE$. The measured phase in the open AB interferometers is in fact the transmission phase, the argument of the transmission amplitudes ($t = |t|e^{i\theta}$). Recent works^{9,12} made clear distinctions between the two phases. In the absence of the transmission zeros, the two phases are identical. The transmission phase jumps by π at the real transmission zeros and the two phases differ by this amount.^{9,10,12} In a time-reversal symmetric system, all the possible transmission zeros are proven to be *real*.^{9,13} For more details about the transmission phase in the time-reversal symmetric case, see the works of Lee⁹ and of Taniguchi and Büttiker.¹²

In this paper, we address the following question: What will happen to the transmission zeros and the transmission

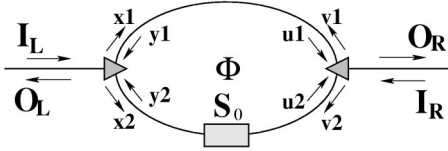


FIG. 1. Aharonov-Bohm ring with an embedded target system. The scattering process in the target system is described by the scattering matrix S_0 . The length of the upper and lower arms is denoted by L . Φ is the magnetic Aharonov-Bohm (AB) flux threading through the AB ring.

phase when the time-reversal symmetry is broken by the external fields, e.g., the magnetic fields? Specifically we answer this question by studying the closed AB ring (see Fig. 1) with an embedded scattering center in the presence of the magnetic AB flux. Since the AB ring provides the transmission zeros due to the destructive interference between two arms and the time-reversal symmetry can be broken by applying the magnetic fields, the AB interferometer is an ideal system for our purpose. In connection to our work, we note that the effects of broken *unitarity* in the AB ring on the phase locking were investigated by another group.¹⁴

In general, either one transmission pole or one transmission zero gives rise to the phase change by π as the Fermi energy is scanned through the real part of the pole or zero. The poles always lie in the lower half plane of the complex-energy plane due to the causality relation. On the other hand, the zeros can be anywhere in the complex-energy plane as we will discuss below when the time-reversal symmetry is broken. Poles give the same contribution to the Friedel phase θ_f and the transmission phase θ_t . The energy scale over which the phase evolution occurs is determined by the imaginary part of the transmission poles. On the other hand, transmission zeros give an additional contribution θ_z only to the transmission phase. The transmission phase can be written as the sum of two: $\theta_t = \theta_f + \theta_z$. Depending on the position of zeros in the complex-energy plane, the behavior of the phase evolution becomes quite different. When the transmission zeros lie on the real-energy axis, an abrupt phase jump by π is observed. Varying the AB magnetic flux, the transmission zeros can be shifted off the real-energy axis. In this case, the transmission phase evolution is continuous and occurs over the energy scale—the imaginary part of transmission zeros—as the Fermi energy is scanned. That is, the transmission phase becomes a discontinuous function of control parameters when the transmission zeros hit the real-energy axis.

To summarize the results of our study, the transmission zeros of t (the transmission amplitude of the closed AB ring), based on their position in the complex-energy plane, can be grouped into three different classes.

Class I: Transmission zeros lie on the real-energy axis. The trajectory of the transmission amplitude t passes through the origin and the transmission phase θ_t jumps by π at the transmission zero.

Class II: Poles and zeros lie in the same lower half-plane of the two-dimensional (2D) complex-energy plane. The trajectory does not encircle the origin, and the evolution of θ_t is

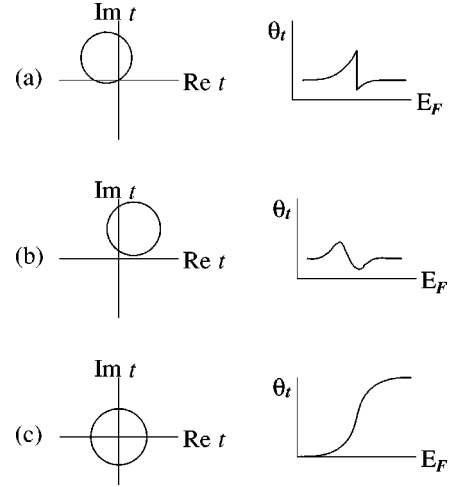


FIG. 2. Schematic display of trajectories of the transmission amplitude t and its phase variation. In the panel (a), the imaginary part of the transmission zero Z_z is null or $\text{Im } Z_z = 0$ (class I). In (b), $\text{Im } Z_z < 0$ (class II), and in (c), $\text{Im } Z_z > 0$ (class III).

continuous and its range is confined by two extreme points of the trajectory when viewed from the origin. Each pole and zero gives rise to the phase change by π , but the sign is opposite. The combined effect of one pole and one zero is a smooth evolution of θ_t and the difference $\Delta\theta_t$ before and after passing through one zero and one pole approaches 0 or $\Delta\theta_t = 0$.

Class III: Poles (zeros) lie in the lower (upper) half plane, respectively. The trajectory encircles the origin. One pole and one zero give the same sign of the phase evolution and $\Delta\theta_t = 2\pi$.

Trajectories of the transmission amplitude t and its phase are schematically shown in Fig. 2 to help the readers to understand three different classes of transmission zeros Z_z . Depending on the nature of the scattering centers which are inserted into one arm of the AB interferometer, all three classes or some of them can be realized by varying magnetic AB flux. We find from our study that the transmission zeros are real when the AB flux is an integer or a half integer multiple of the flux quantum, and the transmission phase jumps by π at the zeros. The transmission zeros become complex or shifted off the real-energy axis when the magnetic AB flux is not an integer or a half integer multiple of the flux quantum, and the transmission phase evolves continuously. The distance of the zeros from the real-energy axis or the imaginary part of the transmission zeros are sinusoidal as function of the magnetic AB phase.

A general formulation on the S matrix for the AB ring is presented in Appendix A when scattering centers are present along the arms of the AB ring. These scattering centers and the accrued phase by the motion along the AB ring can be parametrized by the matrices \mathcal{R} 's and \mathcal{T} 's as described in Appendix A. In this paper, we are interested in the AB ring (see Fig. 1) when the target system is inserted in the lower arm. When the target system is described by the scattering matrix $S_0 = \begin{pmatrix} r_0 & t'_0 \\ t_0 & r'_0 \end{pmatrix}$, the matrices \mathcal{R} 's and \mathcal{T} 's are given by the generic forms,

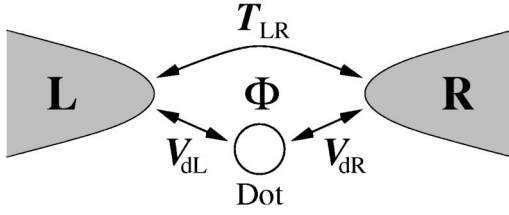


FIG. 3. Schematic display of Aharonov-Bohm (AB) interferometer with a quantum dot. The dot is modeled by one discrete energy level.

$$\begin{aligned} \mathcal{R} &= z_F \begin{pmatrix} 0 & 0 \\ 0 & r_0 \end{pmatrix}, & \mathcal{T} &= z_F \begin{pmatrix} e^{i\phi/2} & 0 \\ 0 & t_0 e^{-i\phi/2} \end{pmatrix}, \\ \mathcal{R}' &= z_F \begin{pmatrix} 0 & 0 \\ 0 & r'_0 \end{pmatrix}, & \mathcal{T}' &= z_F \begin{pmatrix} e^{-i\phi/2} & 0 \\ 0 & t'_0 e^{i\phi/2} \end{pmatrix}. \end{aligned} \quad (2)$$

Here $\phi = 2\pi\Phi \cdot e/hc$ is the AB phase due to the magnetic flux Φ passing through the AB ring. Half of the AB phase is attached to each of the lower and the upper arms of the AB ring. The trajectory of t depends on the chosen gauge or how the AB phase is inserted into the scattering matrix. Of course, the measurable quantities like $|t|^2$ and $\Delta\theta_t$ do not depend on the gauge. $z_F = e^{ik_F L}$ is the phase accrued by the motion of electrons along either of two arms of length L . Since we are interested in a phase-coherent system, we restrict our study to $T=0$ K. The incident electrons will be confined to the Fermi energy with the wave number k_F in our study.

In subsequent sections, we illustrate the effects of broken time-reversal symmetry on the transmission zeros in the AB interferometer by studying three model systems. In Sec. II, we consider the AB interferometer with one discrete energy level. This system is simple enough to obtain the S matrix in a closed form and allows one to study analytically the behavior of the transmission zero under the AB flux. In Secs. III and IV, we study the AB ring when two different types of multiresonant level systems are inserted in the lower arm. In Sec. III, we study the transmission properties of the AB ring with an embedded double-barrier well. The double-barrier well provides multidiscrete energy levels through which the resonant tunneling is realized, but the transmission probability never becomes zero for this system. In Sec. IV, a t stub with the double barrier is inserted in the AB ring. In contrast to the double-barrier well, the t stub accommodates the transmission zeros as well as the multiresonant levels. Our study is summarized in Sec. V.

II. AB INTERFEROMETER WITH AN EMBEDDED RESONANT LEVEL

In this section, we consider the Aharonov-Bohm interferometer shown in Fig. 3. This model system may be the simplest one which can accommodate the zero-pole pair in the transmission amplitude. This system contains both the direct tunneling between two leads and the resonant tunneling through one discrete energy level in the dot. The study of this simple model system helps us to analyze more realistic and

complex systems to be discussed in the subsequent sections. The transmission amplitude of this system is characterized with one pole and one zero. The pole is provided by the discrete level in the dot while the zero is the result of the destructive interference in the AB ring geometry. Three different classes in the trajectories of t , summarized in the introduction, can all be realized with the variation of the AB phase.

We can derive the scattering matrix of the AB interferometer using the t -matrix method with $S_{ij} = \delta_{ij} - 2\pi\delta(E_i - E_j)T_{ij}$ or the Green's-function method,

$$S_{\text{ring}} = \begin{pmatrix} r_{LL} & t_{RL} \\ t_{LR} & r_{RR} \end{pmatrix}, \quad (3)$$

where the reflection and transmission amplitudes are given by the equations

$$t_{RL} = -i\sqrt{T_0} - \bar{\Gamma}G'_d(\epsilon)[\sqrt{T_0} + \sqrt{g}\sin\phi + i\sqrt{g(1-T_0)}\cos\phi], \quad (4a)$$

$$t_{LR} = -i\sqrt{T_0} - \bar{\Gamma}G'_d(\epsilon)[\sqrt{T_0} - \sqrt{g}\sin\phi + i\sqrt{g(1-T_0)}\cos\phi], \quad (4b)$$

$$r_{LL} = \sqrt{1-T_0} - \bar{\Gamma}G'_d(\epsilon) \left[\frac{2i}{1+\gamma} - 2i\frac{\Gamma_R}{\Gamma} + \sqrt{gT_0}\cos\phi \right], \quad (4c)$$

$$r_{RR} = \sqrt{1-T_0} - \bar{\Gamma}G'_d(\epsilon) \left[\frac{2i}{1+\gamma} - 2i\frac{\Gamma_L}{\Gamma} + \sqrt{gT_0}\cos\phi \right]. \quad (4d)$$

The angle ϕ is the Aharonov-Bohm phase $2\pi\Phi/\Phi_0$, where Φ is the magnetic flux threading through the AB ring and $\Phi_0 = hc/e$ is the flux quantum. The gauge is chosen such that the AB phase ϕ is attached to the tunneling matrix V_{dR} as $V_{dR} = |V_{dR}|e^{i\phi}$. $T_0 = 4\gamma/(1+\gamma)^2$ is the direct tunneling probability, where $\gamma = \pi^2 N_L N_R |T_{LR}|^2$. N_L and N_R are the density of states (DOS) in the left and right leads, respectively. Other parameters are defined as $\Gamma_p = \pi N_p |V_{dp}|^2$ ($p = L, R$), $\Gamma = \Gamma_L + \Gamma_R$, $\bar{\Gamma} = \Gamma/(1+\gamma)$, and $g = 4\Gamma_L \Gamma_R / \Gamma^2$.

The S matrix satisfies the Onsager relation, $S_{ij}(\phi) = S_{ji}(-\phi)$, under the inversion of the magnetic flux. If the system is mirror symmetric under the transformation $L \leftrightarrow R$ or the quantum dot is coupled symmetrically to the left and right leads ($\Gamma_L = \Gamma_R$), we obtain the symmetric relation $r_{LL} = r_{RR}$.

The discrete energy level in a dot is broadened with the linewidth Γ due to the coupling to the left and right leads. The direct tunneling between the two leads further renormalizes the linewidth ($\bar{\Gamma}$) and shifts the energy-level position. The retarded Green's function G'_d of a dot is given by the equation

$$G'_d(\epsilon) = \frac{1}{\epsilon - \epsilon_d(\phi) + i\bar{\Gamma}}, \quad (5)$$

Here $\epsilon_d(\phi) = \epsilon_d - \bar{\Gamma} \sqrt{g} \gamma \cos \phi$ is the renormalized energy level of a dot. The transmission probability can be readily calculated from $T(\epsilon) = |t_{RL}|^2$,

$$T(\epsilon) = T_0 + 2\bar{\Gamma} \sqrt{g T_0 (1 - T_0)} \cos \phi \operatorname{Re} G_d^r + \bar{\Gamma} [T_0 - g(1 - T_0 \cos^2 \phi)] \operatorname{Im} G_d^r. \quad (6)$$

The transmission probability $T(\epsilon, \phi)$ is an even function of the AB phase ϕ , satisfying the Onsager relation.

We may rewrite the elements of the scattering matrix in other forms,

$$t_{LR} = -i G_d^r(\epsilon) [\sqrt{T_0}(\epsilon - \epsilon_d) + \bar{\Gamma} \sqrt{g} e^{i\phi}], \quad (7a)$$

$$t_{RL} = -i G_d^r(\epsilon) [\sqrt{T_0}(\epsilon - \epsilon_d) + \bar{\Gamma} \sqrt{g} e^{-i\phi}], \quad (7b)$$

$$r_{LL} = G_d^r(\epsilon) [\sqrt{R_0}(\epsilon - \epsilon_d) - \bar{\Gamma} \sqrt{g} \gamma \cos \phi + i(\bar{\Gamma}_R - \bar{\Gamma}_L)], \quad (7c)$$

$$r_{RR} = G_d^r(\epsilon) [\sqrt{R_0}(\epsilon - \epsilon_d) - \bar{\Gamma} \sqrt{g} \gamma \cos \phi - i(\bar{\Gamma}_R - \bar{\Gamma}_L)]. \quad (7d)$$

Here $R_0 = 1 - T_0$ is the reflection probability of the direct tunneling. Using the above expressions, we can show the unitarity of the S matrix, $|t_{LR}|^2 + |r_{LL}|^2 = 1$ and $r_{LL} t_{LR}^* + t_{RL} r_{RR}^* = 0$.

The Friedel phase θ_f can be found from the determinant of S which can be written in terms of the Green's function of a dot,

$$\det S = \frac{G_d^r}{G_d^a} = \frac{\epsilon - \epsilon_d(\phi) - i\bar{\Gamma}}{\epsilon - \epsilon_d(\phi) + i\bar{\Gamma}} = e^{2i\theta_f}, \quad (8a)$$

$$\theta_f = \frac{\pi}{2} + \tan^{-1} \frac{\epsilon - \epsilon_d(\phi)}{\bar{\Gamma}}. \quad (8b)$$

$G_d^a = [G_d^r]^*$ is the advanced Green's function of a dot. The Friedel phase changes smoothly from $\theta_f = 0$ to $\theta_f = \pi$ as the energy level of a dot is scanned through the Fermi energy.

The transmission phase θ_t is obtained from $t = t_{RL} = |t_{RL}| e^{i\theta_t}$ and is written as the sum of the Friedel phase and the contribution from the zero. Equation (7b) can be written as

$$t = -i \frac{(\epsilon - \epsilon_d) \sqrt{T_0} + \bar{\Gamma} \sqrt{g} \cos \phi - i\bar{\Gamma} \sqrt{g} \sin \phi}{\epsilon - \epsilon_d + \bar{\Gamma} \sqrt{g} \gamma \cos \phi + i\bar{\Gamma}}. \quad (9)$$

The transmission amplitude at the Fermi energy $t(\epsilon=0)$ is plotted in the 2D complex plane in Figs. 4(a) and (d) as an implicit function of ϵ_d while varying the AB phase ϕ . All the trajectories of t are circles. The position of a discrete energy level ϵ_d , which can be shifted with the gate voltage capacitively coupled to the dot, is varied from the empty state to the filled state. That is, the value of ϵ_d is changed from ∞ to $-\infty$. Writing $Z = \epsilon - \epsilon_d$, we can rewrite $t = t_{RL}$ as

$$t = -i \sqrt{T_0} \frac{Z - Z_z}{Z - Z_p}, \quad (10)$$

in terms of the pole Z_p and the zero Z_z . This zero-pole pair is given by the expressions

$$Z_p = -\bar{\Gamma} \sqrt{g} \gamma \cos \phi - i\bar{\Gamma}, \quad (11a)$$

$$Z_z = -\bar{\Gamma} \sqrt{\frac{g}{T_0}} [\cos \phi - i \sin \phi]. \quad (11b)$$

Note that the imaginary part of the transmission zero is proportional to $\sin \phi$ and vanishes when $\phi = n\pi$ (n is an integer).

When the magnetic AB flux is an integer or a half integer multiple of the flux quantum, or when $\phi = n\pi$ (n is an integer), the imaginary part of Z_z vanishes and the transmission zero lies on the real-energy axis. The trajectory of t passes through the origin (the class I). The analytic expression of the transmission phase θ_t when $\phi = n\pi$ is given by the equation

$$\theta_t = \theta_f + \theta_z, \quad (12a)$$

$$\theta_z = \pi - \pi \Theta(\epsilon - \epsilon_d + (-1)^n \bar{\Gamma} \sqrt{g/T_0}). \quad (12b)$$

Here $\Theta(x)$ is the step function. θ_f is the Friedel phase given by Eq. (8b) and θ_z is the contribution from the transmission zero. Since the transmission zero is real, the transmission phase jumps abruptly by π as shown in Figs. 4(b) and (e). The zero-pole pair leads to the typical Fano resonance and antiresonance structure in the transmission amplitude $T = |t|^2$ and $T = 0$ at the antiresonance [see Figs. 6(a) and (f)].

When the magnetic AB flux is off an integer or a half integer multiple of the flux quantum, the imaginary part of the transmission zero is finite and is sinusoidal as function of the AB phase ϕ [see Eq. (11b)]. That is, the zero of t is shifted off the real-energy axis. When $0 < \phi < \pi$, the zero Z_z lies in the upper half plane of the complex-energy plane while the pole Z_p lies in the lower half plane. The trajectories of t encircle the origin (the class III). The analytic expression of θ_t is

$$\theta_t = \theta_f + \tan^{-1} \frac{\epsilon - \epsilon_d + \bar{\Gamma} \sqrt{g/T_0} \cos \phi}{\bar{\Gamma} \sqrt{g/T_0} \sin \phi}. \quad (13)$$

The second term is the contribution from the zero. Since both the zero and the pole contribute the same sign of the phase by π to θ_t , θ_t evolves smoothly by the amount of 2π as shown in Fig. 4(b). The imaginary part of the zero is proportional to $\sin \phi$ and the zero moves away linearly with the magnetic field B from the real-energy axis close to $\phi = n\pi$. The minimum value of T (deriving from the transmission zero) shows this trend as displayed in Fig. 4(c). As ϕ is increased from 0 to $\pi/2$, the minimum value of T_{\min} is increased and reaches the maximum at $\phi = \pi/2$. With further increase of ϕ from $\pi/2$ to π , T_{\min} is reduced to zero.

When $\pi < \phi < 2\pi$, the pole and the zero lie in the same lower half plane. The transmission amplitude, belonging to

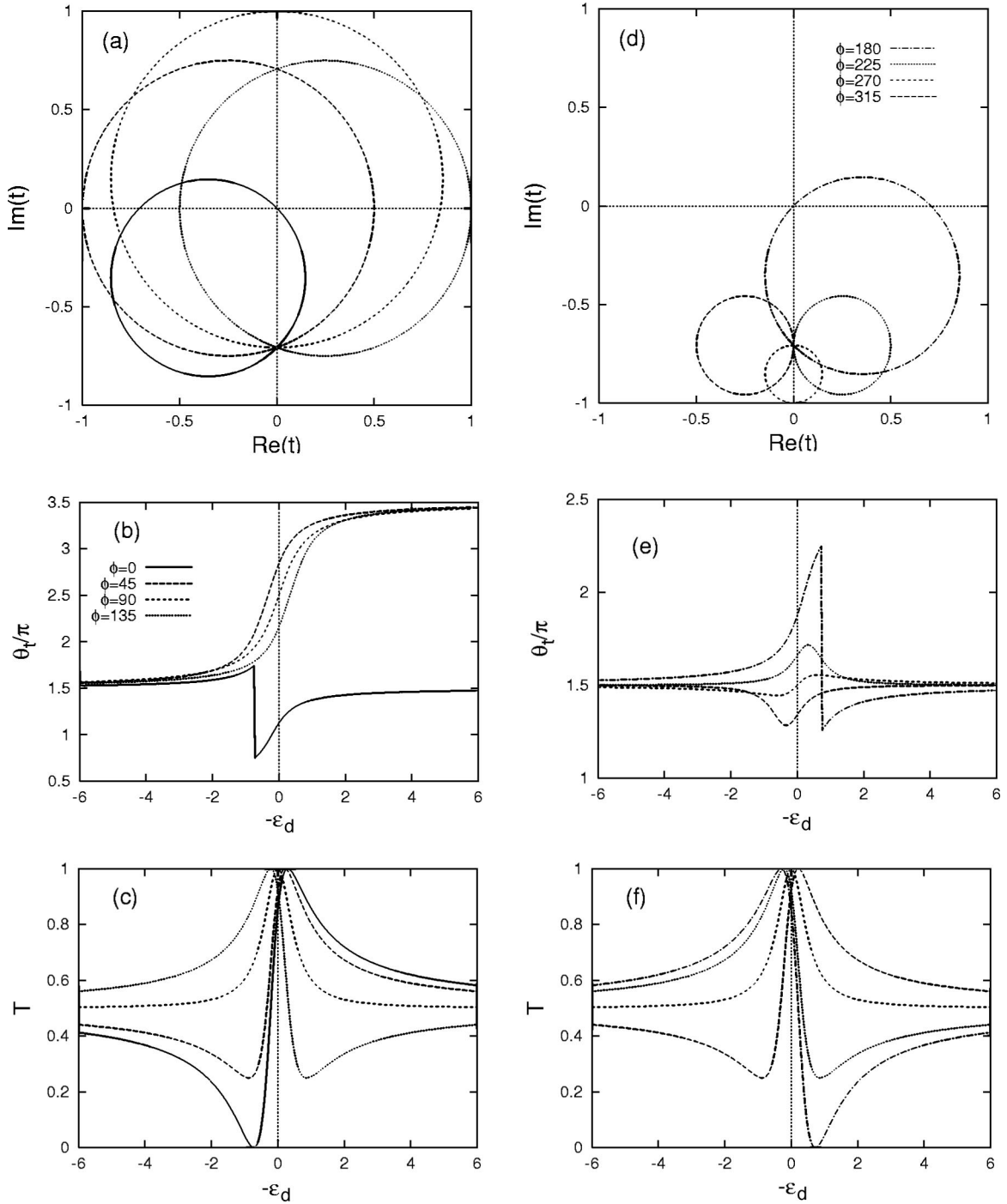


FIG. 4. Behavior of the transmission amplitude t with varying the AB phase ϕ for the AB interferometer with one discrete energy level. Panels (a) and (d) display the trajectories of t as an implicit function of the discrete energy level ϵ_d . The evolution of the transmission phase θ_t is shown in panels (b) and (e). The transmission probability $T=|t|^2$ is displayed in two panels (c) and (f). The AB phases are the same for the same lines either in the left column panels (a), (b), and (c) or in the right column panels (d), (e), and (f).

class II, delineates the closed orbit without encircling the origin. The transmission phase θ_t is given by the expression

$$\theta_t = \theta_f + \pi - \tan^{-1} \frac{\epsilon - \epsilon_d + \bar{\Gamma} \sqrt{g/T_0} \cos \phi}{\bar{\Gamma} \sqrt{g/T_0} \sin \phi}. \quad (14)$$

Since the pole and zero contribute the phase by π but with the opposite sign to θ_t , the phase evolution is limited to the

narrow range [see Fig. 4(e)] which is set by the two extreme points in the trajectory of t viewed from the origin.

In summary, we found three different classes for the transmission zeros. Though the behaviors of the phase evolution are different for the three classes, the transmission amplitudes remain in phase before and after the Fermi level is scanned through the real part of the transmission pole and zero. The transmission probability satisfies the Onsager rela-

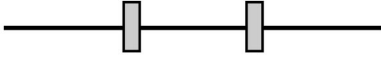


FIG. 5. Double-barrier well.

tion, $|t_{RL}(-\phi)|^2 = |t_{RL}(\phi)|^2$ [see Figs. 4(c) and (f)], even if the trajectories in the complex t plot are different. When the magnetic flux Φ is an integer or a half integer multiples of the flux quantum, the transmission zero lies on the real-energy axis and the phase evolution of θ_t is featured with the abrupt jump by π at the zero. When the magnetic flux Φ is off from the integer values or the half integer multiples of the flux quantum, the transmission zero lies off the real-energy axis and the phase evolution of θ_t becomes continuous over the energy scale $\bar{\Gamma}\sqrt{g}|\sin\phi|$ set by the magnetic fields. Depending on the sign of the imaginary part of the transmission zero, the evolution of θ_t shows different behavior. When the zero lies in the upper half plane, the contributions to the transmission phase from the zero-pole pair add up leading to the change of 2π over the zero-pole pair. On the other hand, two contributions are canceled by each other leading to the net change of 0 in the transmission phase when the zero lies in the lower half plane.

III. AB RING WITH AN EMBEDDED DOUBLE-BARRIER WELL

In this section we study the scattering matrix of the AB ring when the double-barrier well (shown in Fig. 5) is inserted in the lower arm. The symmetric double-barrier well can be described by the scattering matrix S_0 whose elements are given by the equations

$$r_0 = r'_0 = \frac{\sqrt{1-T_0}(1-e^{2iKa})}{1-(1-T_0)e^{2iKa}}, \quad (15a)$$

$$t_0 = t'_0 = \frac{-T_0e^{iKa}}{1-(1-T_0)e^{2iKa}}. \quad (15b)$$

Here $K = \sqrt{k_F^2 + 2meV_g/\hbar^2}$ is the wave number inside the double-barrier well, a is the distance between two barriers, and V_g is the gate voltage capacitatively coupled to the double-barrier well. The position of the resonant energy levels in the double-barrier well is controlled by the gate voltage V_g . The incident electrons are confined to the Fermi level with the Fermi wave number k_F . Two barriers are assumed to be identical and to be described by the scattering matrix

$$S_b = \begin{pmatrix} \sqrt{1-T_0} & -i\sqrt{T_0} \\ -i\sqrt{T_0} & \sqrt{1-T_0} \end{pmatrix}, \quad (16)$$

where T_0 is the tunneling probability through the barrier. The transmission poles of t_0 (double-barrier well) are easily identified as

$$K_p a = n\pi - i\Gamma, \quad \Gamma \equiv \frac{1}{2} \ln \frac{1}{1-T_0}, \quad (17)$$

where n is a positive integer. If the barriers' scattering matrix is of the form given by Eq. (20) in Sec. IV, the poles are shifted by $\pi/2$. We note that t_0 can be expressed as the sum of simple poles,

$$t_0 = -T_0 e^{iKa} \left[\frac{1}{2} + \frac{i}{2} \sum_n \frac{1}{Ka - n\pi + i\Gamma} \right]. \quad (18)$$

The transmission probability $|t_0|^2$ consists of a series of evenly spaced peaks with the same linewidth Γ . Transmission zeros are absent in the double-barrier resonant tunneling system.

We now study the properties of the transmission amplitude for the AB ring with an embedded double-barrier well. Inserting the scattering matrix S_0 of the double-barrier well into the general expression of the S matrix of the AB ring (Appendix A), we compute the transmission amplitude numerically. The results are displayed in Fig. 6. In the numerical works, we use the model parameters: $k_F L = 5\pi/3(2\pi \text{ mod.})$; $\epsilon = 1/2, \lambda_1 = \lambda_2 = 1$ for the identical three-way splitters at the right and left junctions; $T_0 = 0.2$ for the transmission probability of the double-barrier well. One closed orbit in the complex t plot is completed with the variation of $\Delta(Ka) = 2\pi$. In the double-barrier well,¹² the orbit of t is closed with the period 2π of Ka . Comparing our results to the Fig. 1 in the work¹² of Taniguchi and Büttiker, the orbit of t for the AB ring is featured with an additional closed lobe. This lobe passes through the origin when $\phi = 0$ or π . But note that the lobe disappears in t for some range of ϕ . See the dotted line ($\phi = 135^\circ$) in Fig. 6(a) and the long dashed line ($\phi = 315^\circ$) in Fig. 6(d).

When $\phi = 0$ or π , the trajectory of t passes through the origin twice to complete the closed orbit. The transmission phase θ_t jumps by π at the transmission zeros [see the solid line in Fig. 6(b) and the dot-dashed line in Fig. 6(e)] since the transmission zeros are real. The phase increases by π at one zero and decreases by π at the other zero. These two real zeros are typical and behave differently when $\phi \neq 0$ or π , as will be shown later. Each transmission pole of the double-barrier well is paired with one transmission zero in the AB ring. The transmission zeros in the AB ring are the consequence of the destructive interference between two arms. As shown in Figs. 6(c) and (f), the zero-pole pairs are developed in the order zero-zero-pole-pole.

When $\phi \neq 0$ or π , all trajectories of t encircle the origin. These orbits can be considered as the combination of the two orbits: one (class III) encircles the origin while the other (class II) does not. Comparing $|t|^2$ and θ_t between Figs. 4 and 6, we can deduce that the transmission zeros are shifted off the real-energy axis. This point will be discussed later.

Let us study the structure of the poles and the zeros in detail. We focus on the two consecutive zero-pole pairs: one near $Ka = 2\pi$ and the other near $Ka = 3\pi$. These two zeros are typical in the sense that others are the exact copies of these two in the physical properties. The nature of these two zeros is different since they behave in the opposite way under the magnetic fields (see Fig. 7.) When $\phi = 0$, we can deduce from Figs. 6(b) and (c) that the zero-pole pairs are ordered in the sequence pole-zero-zero-pole. When $0 < \phi$

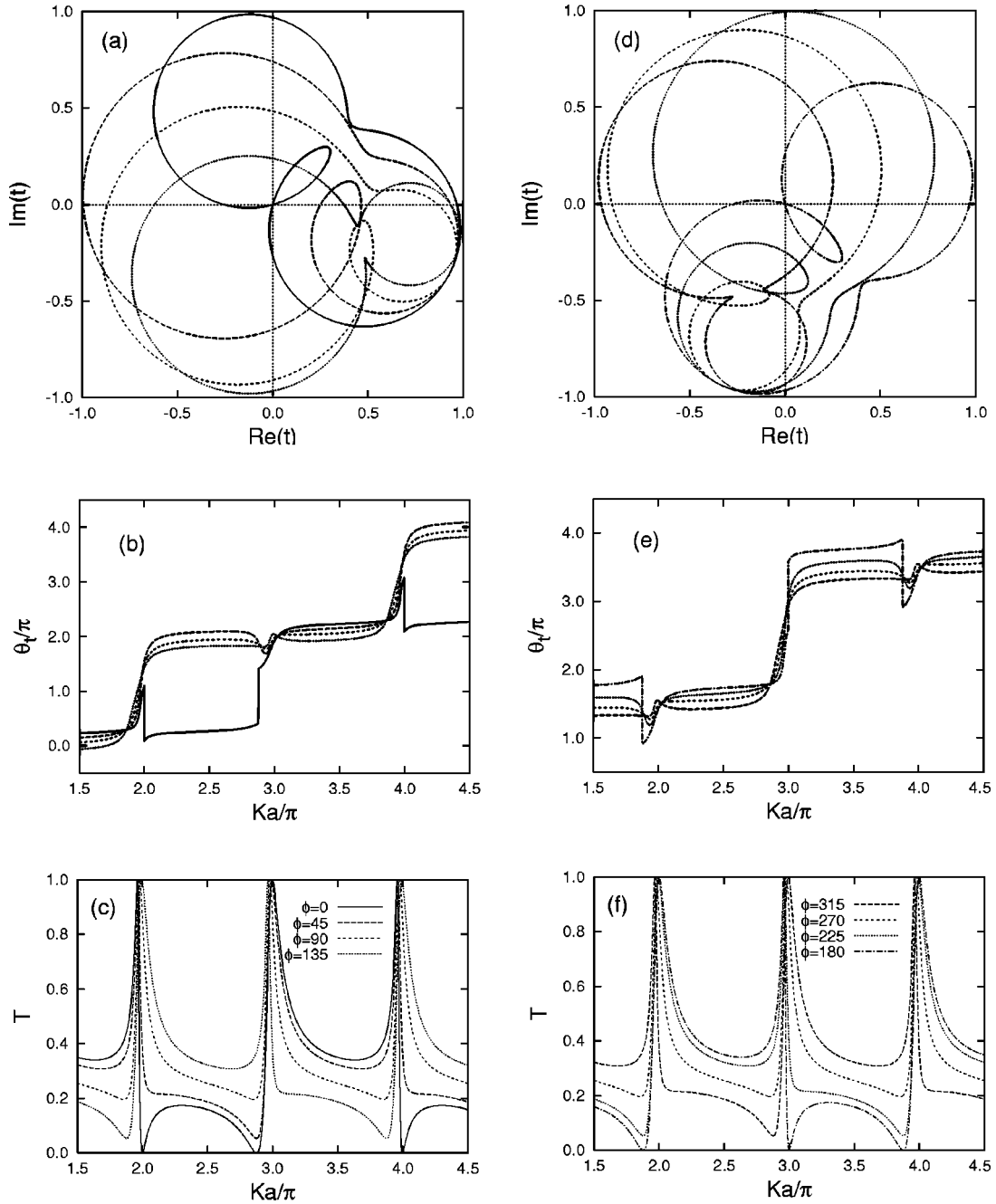


FIG. 6. Behavior of the transmission amplitude t with varying the AB phase ϕ for the AB ring with the double-barrier well. Panel descriptions are the same as in Fig. 4. Model parameters are chosen as $k_F L = 5\pi/3 \pmod{2\pi}$, $\epsilon_{L,R} = 1/2$, $\lambda_1 = \lambda_2 = 1$ and $T_0 = 0.2$.

$< \pi$, we conclude, using the results of Sec. II, for the zero-pole pair near $Ka = 2\pi$ that the zero (pole) lies in the upper (lower) half plane of the complex-energy plane, respectively. On the other hand, the zero-pole pair near $Ka = 3\pi$ is in the lower half plane. This is the reason why the phase change is 2π over the first zero-pole pair and is 0 over the second zero-pole pair. When $\phi = \pi$, the zero-pole pairs appear in the sequence zero-pole-pole-zero. When $\pi < \phi < 2\pi$, the roles of two aforementioned zero-pole pairs are interchanged compared to the case of $0 < \phi < \pi$.

We compute the traces of the transmission zeros $Z_z(\phi)$ in the complex-energy plane ($z = Ka$) as function of the magnetic AB phase ϕ .

$$Z_z(\phi) = E_z + \zeta(\phi). \quad (19)$$

Here E_z is the transmission zero when $\phi = 0$ and $\zeta(\phi)$ is the shift of the zero in the presence of the magnetic AB flux. There are two distinct zeros in the AB ring with the double-barrier well and the behavior of two zeros is different under the magnetic AB flux. The real and the imaginary parts of $\zeta(\phi)$ are plotted in Fig. 7 for two zeros of $E_z = Ka = 2\pi$ [panel (a)] and of $E_z = Ka \approx 2.8775 \times \pi$ [panel (b)]. The real part of the first (second) zero is shifted downward (upward) under the magnetic fields, respectively. The minimum in $T = |t|^2$ [see Figs. 6(c) and (e)] shows this trend. The two zeros

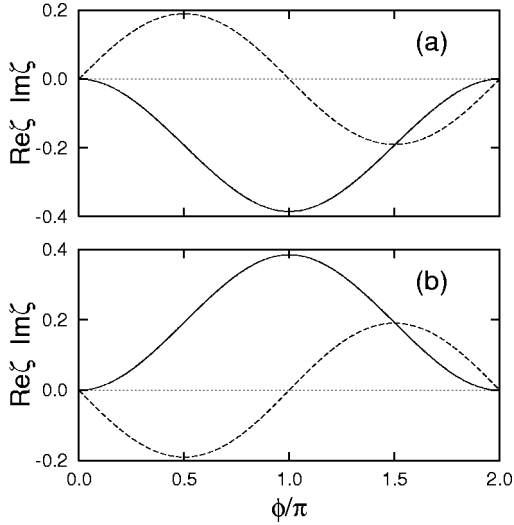


FIG. 7. Transmission zeros as function of the AB phase ϕ in the AB ring with the double-barrier well. The AB phase dependence of the zero at $Ka = 2\pi [2.8775 \times \pi]$ is displayed in panel (a) [(b)], respectively. Solid (dashed) line is the real (imaginary) part of the shifted zero $\zeta(\phi)$, respectively. The transmission zero is represented by $Z_z(\phi) = E_z + \zeta(\phi)$ where E_z is the transmission zero when $\phi = 0$ and $\zeta(\phi)$ is the shift of the zero in the presence of the magnetic AB flux.

show the opposite behavior in their imaginary parts under the magnetic fields, too. The zero $E_z = 2\pi(2.8775 \times \pi)$ lies in the upper (lower) half plane when $0 < \phi < \pi$, and in the lower (upper) half plane when $\pi < \phi < 2\pi$, respectively. This corroborates our conclusion in the previous paragraph. Two zeros are on the real-energy axis when $\phi = n\pi$ with n being an integer.

To summarize, there are two types of the transmission zeros which can be distinguished in their behavior under magnetic fields. Since one pole is always paired with one zero, the change in the transmission phase over the zero-pole pair is 0 or 2π depending on the position of the zero in the complex-energy plane.

IV. AB INTERFEROMETER WITH AN EMBEDDED t STUB

In this section, we consider the AB ring with the side branch or the t stub. The t stub provides the different type of resonant levels compared to the double-barrier well. In contrast to the double-barrier well, the t stub itself provides the transmission zeros as well as the transmission poles. In this work, we consider the t -stub structure with two tunneling barriers which was previously studied in the literature.^{10,15} We use the most symmetric three-way splitter at the junction with the parameters¹⁵ $\epsilon = 4/9$, $\lambda_1 = -1$, and $\lambda_2 = 1$. The double-barrier is assumed not to provide any resonant energy levels, or the distance between two barriers is so short that the energy-level spacing is much larger than any other interesting energy scale in the problem. The introduction of two additional barriers to the t stub enables us to control the tunneling strength through the t -stub structure and to mimic

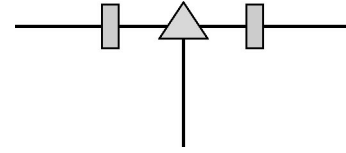


FIG. 8. t stub with the double barrier.

the quantum dot system. The S matrix of the two barriers is chosen to be

$$S_b = \begin{pmatrix} i\sqrt{1-T_0} & \sqrt{T_0} \\ \sqrt{T_0} & i\sqrt{1-T_0} \end{pmatrix}, \quad (20)$$

where T_0 is the tunneling probability through the barrier. We have chosen the different overall phase for S_b compared to the double-barrier well in Sec. III. The S matrix of the t stub with the double barriers is formulated in Appendix B (see Fig. 8).

To get some insights on the position of the transmission zeros and poles, we consider the S matrix of the simple t stub. The incoming and outgoing current amplitudes can be matched at the junction of the t stub,

$$\begin{pmatrix} O_S \\ O_L \\ O_R \end{pmatrix} = \begin{pmatrix} \sigma_t & \sqrt{\epsilon_t} & \sqrt{\epsilon_t} \\ \sqrt{\epsilon_t} & a_t & b_t \\ \sqrt{\epsilon_t} & b_t & a_t \end{pmatrix} \begin{pmatrix} I_S \\ I_L \\ I_R \end{pmatrix}. \quad (21)$$

Here I 's and O 's are the incoming and outgoing current amplitudes at the junction. $\sigma_t = -a_t - b_t$ and a_t, b_t can be determined to satisfy the unitarity of the scattering matrix,

$$a_t = \frac{1}{2}[\lambda_1 + \lambda_2 \sqrt{1 - 2\epsilon_t}], \quad (22a)$$

$$b_t = \frac{1}{2}[-\lambda_1 + \lambda_2 \sqrt{1 - 2\epsilon_t}]. \quad (22b)$$

There are four possible choices with $\lambda_i = \pm 1$ ($i = 1, 2$). The value of ϵ_t is constrained: $0 \leq \epsilon_t \leq 1/2$. When there is an infinite potential wall at the end of the stub of length a , O_S and I_S are related to each other by $I_S = O_S e^{i(2Ka + \pi)}$. The additional phase π guarantees the node of the wave function at the infinite wall. The wave number K in the stub is given by $K = \sqrt{k_F^2 + 2meV_g/\hbar^2}$. The quasibound-state energy levels in the stub can be shifted with the gate voltage V_g (capacitively coupled to the t stub). The effective S matrix of the t stub can be readily derived,

$$\begin{pmatrix} O_L \\ O_R \end{pmatrix} = S_0 \begin{pmatrix} I_L \\ I_R \end{pmatrix}, \quad S_0 = \begin{pmatrix} r_0 & t_0 \\ t_0 & r_0 \end{pmatrix}, \quad (23a)$$

$$t_0 = b_t - \frac{\epsilon_t z}{1 + \sigma_t z} = \frac{b_t(1 + \lambda_1 z)}{1 - (a_t + b_t)z}, \quad (23b)$$

$$r_0 = a_t - \frac{\epsilon_t z}{1 + \sigma_t z} = \frac{a_t(1 - \lambda_1 z)}{1 - (a_t + b_t)z}. \quad (23c)$$

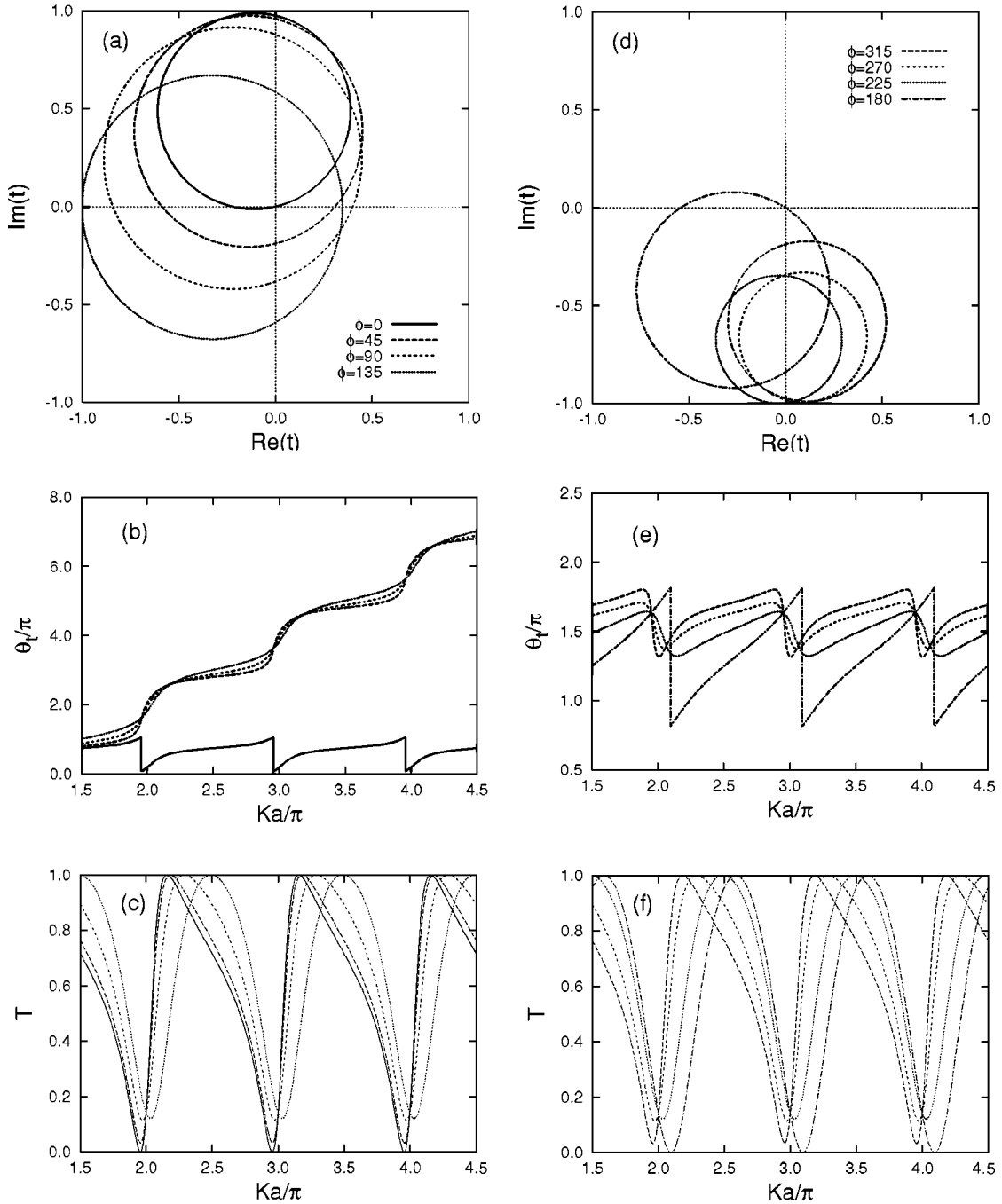


FIG. 9. Behavior of the transmission amplitude t with varying the AB phase ϕ for the AB ring with the t stub. Panel descriptions are the same as in Fig. 4. Model parameters are chosen as $k_F L = \pi/2$; $\epsilon_{L,R} = 1/2$, $\lambda_{L,R1} = -1$, and $\lambda_{L,R2} = 1$; $\epsilon_t = 4/9$, $\lambda_{t1} = -1$, and $\lambda_{t2} = 1$; $T_L = T_R = 0.8$.

Here $z = e^{2iKa}$. The first terms in t_0 and r_0 represent the direct-scattering process and the second term comes from the multiple-scattering processes in the stub. The unitarity of S_0 can be proved by showing that

$$|r_0|^2 + |t_0|^2 = 1, \quad t_0^* r_0 + r_0^* t_0 = 0. \quad (24)$$

The transmission poles and zeros are located at

$$Z_z = \left(n + \frac{1 + \lambda_1}{4} \right) \pi, \quad (25a)$$

$$Z_p = \left(n + \frac{1 - \lambda_2}{4} \right) \pi - \frac{i}{2} \ln \frac{1}{\sqrt{1 - 2\epsilon_t}}, \quad (25b)$$

respectively. Here n is an integer. For our choice of $\lambda_1 = -1$ and $\lambda_2 = 1$ for the t stub, $Z_z = n\pi$ and $\text{Re} Z_p = n\pi$.

The scattering matrix of the t stub with the double barrier is derived in Appendix B. Note that addition of the two barriers to the t stub does not change the transmission zeros, but the poles are modulated by T_0 in both the real and the imaginary parts.

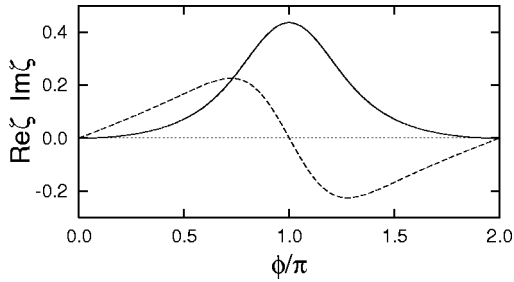


FIG. 10. Transmission zeros as a function of the AB phase ϕ in the AB ring with the t -stub system. Solid (dashed) line is the real (imaginary) part of the shifted zero $\zeta(\phi)$, respectively.

The transmission amplitudes of the whole AB ring are computed numerically using the formulation detailed in Appendixes A and B and are presented in Fig. 9. The model parameters are: $\epsilon=1/2$, $\lambda_1=-1$, and $\lambda_2=1$ for the Shapiro matrices at the left and right three-way junctions. The three-way splitter for the t stub was chosen to be the most symmetric one as noted above. The tunneling barriers for the t stub are chosen as $T_0=0.8$.

As can be deduced from Figs. 9(c) and (f), the zero-pole pairs appear in the order zero-pole-zero-pole. All the trajectories of t are circles and the closed orbit is completed with $\Delta Ka=\pi$. Three different classes of orbits of t are realized for this system varying the magnetic AB flux.

When $\phi=0$ or $\phi=\pi$, the transmission zero lies on the real-energy axis and the transmission phase jumps by π at the zeros. When $\phi=0$, θ_t near $Ka=2\pi$ drops by π at the zero and increases smoothly by the amount π due to the pole. For this zero-pole pair, the zero precedes the pole as shown in Figs. 9(b) and (c). When $\phi=\pi$, θ_t drops by π at the zero and increases almost linearly due to the pole. We can deduce from the functional shape of the θ_t and $T=|t|^2$ [see Figs. 9(e) and (f)] that the zeros and poles are almost evenly interlaced.

When $0<\phi<\pi$, the orbits of t encircle the origin and the phase evolution of θ_t is smooth and continuous. The orbits move away from the origin with increasing the AB phase. This trend is clearly visible in Figs. 9(a) and (c). Since the zeros lie in the upper half plane and the poles are in the lower half plane, two contributions to θ_t add up and lead to the change of θ_t by 2π over the zero-pole pair.

The orbits of t lie outside the origin when $\pi<\phi<2\pi$. In this case, the zeros and the poles lie in the same lower half plane. Their contributions to the transmission phase are opposite in sign, and the net change of θ_t over the zero-pole pair is zero. Since the phase decrease precedes the phase increase, the zero precedes the pole. The zero-pole pair approaches each other as the value of ϕ is increased from π to 2π .

The trace of one typical transmission zero $Z_z(\phi)$ in the complex-energy plane ($z=Ka$) is computed and plotted in Fig. 10 as function of the magnetic AB phase ϕ .

$$Z_z(\phi) = E_z + \zeta(\phi). \quad (26)$$

Here E_z is the transmission zero when $\phi=0$ and $\zeta(\phi)$ is the shift of the zero in the presence of the magnetic AB flux. In

contrast to the AB ring with the double-barrier well, the nature of all zeros is identical in the sense that their behavior is the same under the magnetic fields. The real and imaginary parts of $\zeta(\phi)$ are plotted in Fig. 10 for the zero of $E_z=Ka \approx 1.9565 \times \pi$. Note that this zero in the AB ring is shifted from $E_z=2\pi$ of the t stub with the double barrier. As expected from the shift of the minimum position of $T=|t|^2$ [see Figs. 9(c) and (e)], the real part of the zero is positively shifted in the presence of the magnetic fields. The imaginary part of the zero is sinusoidal as function of the AB phase ϕ and vanishes when the magnetic AB flux is an integer or a half integer multiple of the flux quantum.

V. SUMMARY AND CONCLUSION

In this paper, we studied the behavior of the transmission zeros and the corresponding changes in the transmission phase when the time-reversal symmetry of the system is broken by magnetic fields. For our study we considered the Aharonov-Bohm (AB) interferometers with one scattering center in the lower arm. Studied scattering centers include the system of one discrete energy level, the double-barrier well, and the t stub with the double barriers. Each resonant level in the scattering center gives rise to a transmission pole and is paired with a transmission zero in the AB ring. Due to the causality relation, the transmission pole always lies in the lower half plane of the complex-energy plane. On the other hand, the zero can be anywhere in the complex-energy plane and its position can be controlled by the magnetic AB flux. Depending on the position of the transmission zeros in the complex-energy plane, the trajectory and the phase of the transmission amplitude show different behaviors.

The transmission zeros lie on the real-energy axis when the magnetic AB flux is an integer or a half integer multiple of the flux quantum. The transmission phase jumps by π at the transmission zeros in this case.

The transmission zeros are shifted off the real-energy axis and can be either in the upper or in the lower half plane of the complex-energy plane, when the AB magnetic flux is off from the integer or the half integer multiples of the flux quantum. The evolution of the transmission phase in this case is continuous as the Fermi level is scanned through the real part of the transmission zeros.

When the zeros lie in the lower half plane, the orbits of the transmission amplitude lie outside the origin and the phase change is limited by the two extreme points of the orbit when viewed from the origin. Since the zero-pole pair contributes the opposite sign of the phase by π , the net change in the transmission phase over the zero pole is zero.

The orbits of the transmission amplitude encircle the origin when the zeros lie in the upper half plane. In this case, the zero-pole pair gives the same sign of the phase by π to the transmission phase; the total accrued phase over this zero-pole pair is 2π . Though the zero-pole pair leads to a different phase evolution depending on the position of the zero in the complex-energy plane, the transmission phase remains in phase after passing through the zero-pole pair.

The modulation of the transmission zeros in the closed AB ring may be tested in experiments using the following

setup. We may insert the closed AB ring into one arm of the larger AB ring. The larger AB ring should be the open system where the multiple windings of the electrons are prevented. The evolution of the transmission phase in the closed AB ring can be measured by making the period of the AB oscillation in the larger ring much shorter than that of the closed AB ring.

Entin-Wohlman *et al.*¹⁴ studied the effects of broken unitarity on the phase locking. According to their study, the phase jump at the Coulomb peaks can become smooth by breaking the unitarity of the AB ring. In our work, the phase jump at the transmission zeros is shown to become continuous by breaking the time-reversal symmetry. Recently, Kobayashi *et al.*¹⁶ studied experimentally the tuning of the Fano effect in the AB ring with an embedded quantum dot. Some of their results might be relevant to our theoretical results.

ACKNOWLEDGMENTS

We are indebted to H. W. Lee for useful discussions. This work was supported in part by the BK21 project and in part by Grant No. 1999-2-114-005-5 from the KOSEF and by the Center for Strongly Correlated Materials Research (SNU) from the KOSEF.

APPENDIX A: S MATRIX OF AHARONOV-BOHM RING

In this appendix, we derive the S matrix of an AB ring in a compact form when some scattering centers are present on the AB ring and especially when the interesting target system is inserted in the lower arm of the AB ring as shown in Fig. 1. The amplitudes of the incoming and outgoing waves at the left and right junctions are related to each other by the scattering matrix,

$$\begin{pmatrix} O_L \\ x_1 \\ x_2 \end{pmatrix} = S^L \begin{pmatrix} I_L \\ y_1 \\ y_2 \end{pmatrix}, \quad \begin{pmatrix} O_R \\ v_1 \\ v_2 \end{pmatrix} = S^R \begin{pmatrix} I_R \\ u_1 \\ u_2 \end{pmatrix}, \quad (\text{A1a})$$

$$S^p = \begin{pmatrix} \sigma_p & \sqrt{\epsilon_p} & \sqrt{\epsilon_p} \\ \sqrt{\epsilon_p} & a_p & b_p \\ \sqrt{\epsilon_p} & b_p & a_p \end{pmatrix}, \quad p=L,R. \quad (\text{A1b})$$

Here $S^{L,R}$ are the Shapiro matrices responsible for the splitting of the electron wave functions in three pathways. The unitarity leads to four possible solutions,

$$\sigma_p = -a_p - b_p, \quad (\text{A2a})$$

$$a_p = \frac{1}{2} [\lambda_1^p + \lambda_2^p \sqrt{1 - 2\epsilon_p}], \quad (\text{A2b})$$

$$b_p = \frac{1}{2} [-\lambda_1^p + \lambda_2^p \sqrt{1 - 2\epsilon_p}], \quad (\text{A2c})$$

where $\lambda_1^p, \lambda_2^p = \pm 1$. To simplify the algebra, we introduce new notations,

$$S_p \equiv \begin{pmatrix} a_p & b_p \\ b_p & a_p \end{pmatrix}, \quad |s_p\rangle \equiv \begin{pmatrix} \sqrt{\epsilon_p} \\ \sqrt{\epsilon_p} \end{pmatrix}. \quad (\text{A3})$$

$S_{L,R}$ is the 2×2 submatrix of $S^{L,R}$, respectively. The amplitudes of waves at the left and right junctions are related to each other by the scattering matrix which is responsible for the scattering processes in the two arms,

$$\begin{pmatrix} |y\rangle \\ |u\rangle \end{pmatrix} = \begin{pmatrix} \mathcal{R} & \mathcal{T}' \\ \mathcal{T} & \mathcal{R}' \end{pmatrix} \begin{pmatrix} |x\rangle \\ |v\rangle \end{pmatrix}. \quad (\text{A4})$$

The ket vectors are defined, e.g., as $|x\rangle \equiv \begin{pmatrix} x_1 \\ x_2 \end{pmatrix}$. \mathcal{R} and \mathcal{T} are the 2×2 matrices which contain the information of the scattering matrices in each arm and the phase accrued by the motion of electrons along the ring. These matrices are model specific and are discussed in the main text. We want to find the S matrix of the ring,

$$O_L = \sigma_L I_L + \langle s_L | y \rangle, \quad (\text{A5a})$$

$$O_R = \sigma_R I_R + \langle s_R | u \rangle, \quad (\text{A5b})$$

$$|x\rangle = I_L |s_L\rangle + S_L |y\rangle, \quad (\text{A5c})$$

$$|v\rangle = I_R |s_R\rangle + S_R |u\rangle. \quad (\text{A5d})$$

From the above equations, it is straightforward to derive the following results:

$$|y\rangle = I_L \cdot [1 - \bar{\mathcal{R}} S_L]^{-1} \bar{\mathcal{R}} |s_L\rangle + I_R \cdot [1 - \bar{\mathcal{R}} S_L]^{-1} \bar{\mathcal{T}}' |s_R\rangle, \quad (\text{A6a})$$

$$|u\rangle = I_L \cdot [1 - \bar{\mathcal{R}}' S_R]^{-1} \bar{\mathcal{T}} |s_L\rangle + I_R \cdot [1 - \bar{\mathcal{R}}' S_R]^{-1} \bar{\mathcal{R}}' |s_R\rangle, \quad (\text{A6b})$$

where newly defined reflection and transmission matrices are given by the expressions

$$\bar{\mathcal{R}} = \mathcal{R} + \mathcal{T}' [1 - S_R \mathcal{R}']^{-1} S_R \mathcal{T}, \quad (\text{A7a})$$

$$\bar{\mathcal{T}} = \mathcal{T} [1 - S_L \mathcal{R}]^{-1}, \quad (\text{A7b})$$

$$\bar{\mathcal{R}}' = \mathcal{R}' + \mathcal{T} [1 - S_L \mathcal{R}]^{-1} S_L \mathcal{T}', \quad (\text{A7c})$$

$$\bar{\mathcal{T}}' = \mathcal{T}' [1 - S_R \mathcal{R}']^{-1}. \quad (\text{A7d})$$

After more algebra, we find the S matrix of the ring,

$$\begin{pmatrix} O_L \\ O_R \end{pmatrix} = S_{\text{ring}} \begin{pmatrix} I_L \\ I_R \end{pmatrix}, \quad (\text{A8a})$$

$$S_{\text{ring}} = \begin{pmatrix} r_{LL} & t_{LR} \\ t_{RL} & r_{RR} \end{pmatrix}, \quad (\text{A8b})$$

$$r_{LL} = \sigma_L + \langle s_L | [1 - \bar{\mathcal{R}} S_L]^{-1} \bar{\mathcal{R}} |s_L\rangle, \quad (\text{A8c})$$

$$r_{RR} = \sigma_R + \langle s_R | [1 - \bar{\mathcal{R}}' S_R]^{-1} \bar{\mathcal{R}}' |s_R\rangle, \quad (\text{A8d})$$

$$t_{LR} = \langle s_L | [1 - \bar{\mathcal{R}} S_L]^{-1} \bar{\mathcal{T}}' |s_R\rangle, \quad (\text{A8e})$$

$$t_{RL} = \langle s_R | [1 - \bar{R}' S_R]^{-1} \bar{T} | s_L \rangle. \quad (\text{A8f})$$

APPENDIX B: SCATTERING MATRIX OF THE t -STUB WITH DOUBLE BARRIERS

We consider the S matrix of the t stub with the double barriers (see Fig. 8). The distance between two barriers is assumed to be too short to allow the resonant energy levels, or the energy-level spacing is very large compared to other energy scales. But the length of the stub a is long enough to allow the quantized energy levels in the isolated stub. In this case, the amplitude of the wave functions can be matched as

$$\begin{pmatrix} O_S \\ x_1 \\ x_2 \end{pmatrix} = S^t \begin{pmatrix} I_S \\ y_1 \\ y_2 \end{pmatrix}, \quad S^t = \begin{pmatrix} \sigma & \sqrt{\epsilon} & \sqrt{\epsilon} \\ \sqrt{\epsilon} & a & b \\ \sqrt{\epsilon} & b & a \end{pmatrix}, \quad (\text{B1a})$$

$$\begin{pmatrix} O_L \\ y_1 \end{pmatrix} = S_L \begin{pmatrix} I_L \\ x_1 \end{pmatrix}, \quad \begin{pmatrix} O_R \\ y_2 \end{pmatrix} = S_R \begin{pmatrix} I_R \\ x_2 \end{pmatrix},$$

$$S_p = \begin{pmatrix} r_p & t'_p \\ t_p & r'_p \end{pmatrix}, \quad p = L, R. \quad (\text{B1b})$$

We want to find the S matrix of the t stub with the double barriers,

$$\begin{pmatrix} O_L \\ O_R \end{pmatrix} = S \begin{pmatrix} I_L \\ I_R \end{pmatrix}. \quad (\text{B2})$$

When there is an infinite potential wall at the end of the stub, two amplitudes I_s and O_s are constrained as $I_s = e^{i(2Ka + \pi)} O_s$. We can rewrite the above relations between the amplitudes as

$$O_s = \sigma I_s + \langle s_t | y \rangle, \quad (\text{B3a})$$

$$|x\rangle = I_s |s_t\rangle + S_t |y\rangle, \quad (\text{B3b})$$

$$|O\rangle = R |I\rangle + T' |x\rangle, \quad (\text{B3c})$$

$$|y\rangle = T |I\rangle + R' |x\rangle. \quad (\text{B3d})$$

New notations are introduced to simplify the algebra:

$$|x\rangle = \begin{pmatrix} x_1 \\ x_2 \end{pmatrix}, \quad |y\rangle = \begin{pmatrix} y_1 \\ y_2 \end{pmatrix}, \quad (\text{B4a})$$

$$|I\rangle = \begin{pmatrix} I_L \\ I_R \end{pmatrix}, \quad |O\rangle = \begin{pmatrix} O_L \\ O_R \end{pmatrix}, \quad (\text{B4b})$$

$$|s_t\rangle = \begin{pmatrix} \sqrt{\epsilon} \\ \sqrt{\epsilon} \end{pmatrix}, \quad S_t = \begin{pmatrix} a & b \\ b & a \end{pmatrix}, \quad (\text{B4c})$$

$$R = \begin{pmatrix} r_L & 0 \\ 0 & r_R \end{pmatrix}, \quad T = \begin{pmatrix} t_L & 0 \\ 0 & t_R \end{pmatrix},$$

$$R' = \begin{pmatrix} r'_L & 0 \\ 0 & r'_R \end{pmatrix}, \quad T' = \begin{pmatrix} t'_L & 0 \\ 0 & t'_R \end{pmatrix}. \quad (\text{B4d})$$

From the relation between I_s and O_s , we find

$$\begin{aligned} I_s &= -\frac{1}{\sigma + e^{-2iKa}} \langle s_t | y \rangle \\ &= -\frac{\langle s_t | [1 - R' S_t]^{-1} T | I \rangle}{\sigma + e^{-2iKa} + \langle s_t | [1 - R' S_t]^{-1} R' | s_t \rangle}. \end{aligned} \quad (\text{B5})$$

After some algebra, we find the S matrix of the system $|O\rangle = S_0 |I\rangle$,

$$\begin{aligned} S_0 &= R + T' [1 - S_t R']^{-1} S_t T \\ &\quad - \frac{T' [1 - S_t R']^{-1} |s_t\rangle \langle s_t| [1 - R' S_t]^{-1} T}{\sigma + e^{-2iKa} + \langle s_t | [1 - R' S_t]^{-1} R' | s_t \rangle}. \end{aligned} \quad (\text{B6})$$

Note that the transmission poles are determined by the zeros of $\sigma + e^{-2iKa} + \langle s_t | [1 - R' S_t]^{-1} R' | s_t \rangle$.

For the two identical barriers described by the scattering matrix ($R_0 = 1 - T_0$),

$$S_b = \begin{pmatrix} i\sqrt{R_0} & \sqrt{T_0} \\ \sqrt{T_0} & i\sqrt{R_0} \end{pmatrix}, \quad (\text{B7})$$

the scattering matrix of the t stub with double barrier is given by the equations

$$S_0 = \begin{pmatrix} r_0 & t_0 \\ t_0 & r_0 \end{pmatrix}, \quad (\text{B8a})$$

$$t_0 = \frac{T_0 b}{(1 - i\sqrt{R_0}a)^2 + R_0 b^2} \frac{e^{-2iKa + \lambda_1}}{e^{-2iKa} + \frac{\sigma + i\sqrt{R_0}}{1 + i\sqrt{R_0}\sigma}}, \quad (\text{B8b})$$

$$\begin{aligned} r_0 &= i\sqrt{R_0} + \frac{T_0}{1 + i\sqrt{R_0}\sigma} \cdot \left[\frac{a + i\sqrt{R_0}(b^2 - a^2)}{1 - i\sqrt{R_0}(a - b)} \right. \\ &\quad \left. - \frac{\epsilon}{(1 + i\sqrt{R_0}\sigma)e^{-2iKa} + \sigma + i\sqrt{R_0}} \right]. \end{aligned} \quad (\text{B8c})$$

Note that the transmission zeros do not depend on or are not modified by the barriers' tunneling strength T_0 [see Eqs. (23b) and (25a)], but the poles are modulated by the value of T_0 . The transmission poles (Z_p) and zeros (Z_z) are located at

$$Z_z = \left(n + \frac{1 + \lambda_1}{4} \right) \pi, \quad (\text{B9a})$$

$$Z_p = \left(n + \frac{1 - \lambda_2}{4} \right) \pi + \frac{\lambda_2}{2} \left[\tan^{-1} \sqrt{\frac{R_0}{1 - 2\epsilon}} - \tan^{-1} \sqrt{R_0(1 - 2\epsilon)} \right] - \frac{i}{2} \ln \sqrt{\frac{1 + R_0(1 - 2\epsilon)}{1 - 2\epsilon + R_0}}. \quad (\text{B9b})$$

As expected, the linewidth of quasibound states in the stub (or the imaginary part of poles) is reduced with the reduced T_0 .

¹A. Yacoby, M. Heiblum, D. Mahalu, and H. Shtrikman, Phys. Rev. Lett. **74**, 4047 (1995).

²R. Schuster, E. Buks, M. Heiblum, D. Mahalu, V. Umansky, and H. Shtrikman, Nature (London) **385**, 417 (1997).

³E. Buks, R. Schuster, M. Heiblum, D. Mahalu, V. Umansky, and H. Shtrikman, Phys. Rev. Lett. **77**, 4664 (1996).

⁴W. G. van der Wiel, S. De Franceschi, T. Fujisawa, J. M. Elzerman, S. Tarycha, and L. P. Kouwenhoven, Science **289**, 2105 (2000).

⁵Y. Ji, M. Heiblum, D. Sprinzak, D. Mahalu, and H. Shtrikman, Science **290**, 779 (2000).

⁶M. Büttiker, Phys. Rev. Lett. **57**, 1761 (1986).

⁷A. L. Yeyati and M. Büttiker, Phys. Rev. B **52**, 14 360 (1995).

⁸L. Onsager, Phys. Rev. **38**, 2265 (1931).

⁹H.-W. Lee, Phys. Rev. Lett. **82**, 2358 (1999).

¹⁰C. M. Ryu and S. Y. Cho, Phys. Rev. B **58**, 3572 (1998).

¹¹D. C. Langreth, Phys. Rev. **150**, 516 (1966).

¹²T. Taniguchi and M. Büttiker, Phys. Rev. B **60**, 13 814 (1999).

¹³H.-W. Lee, J. Korean Phys. Soc. **34**, S180 (1999).

¹⁴O. Entin-Wohlman, A. Aharony, Y. Imry, Y. Levinson, and A. Schiller, Phys. Rev. Lett. **88**, 166801 (2002).

¹⁵Z. Shao, W. Porod, and C. S. Lent, Phys. Rev. B **49**, 7453 (1994).

¹⁶K. Kobayashi, H. Aikawa, S. Katsumoto, and Y. Iye, cond-mat/0202006 (unpublished).